International Journal Of
Industrial Electronics Control and Optimization
Print ISSN: 3517-2645
Online ISSN: 3568-2645
Homepage: https://ieco.usb.ac.ir/

# Bidirectional High-Efficiency Converter Based on the Capacitive Wireless Power Transfer Technique for Electric Vehicle Charging and Energy Storage Application

Jasem Shahsevani | Reza Beiranvand

Faculty of Electrical and Computer Engineering, Tarbiat Modares University, Tehran, Iran.[1,2]
Corresponding author's email: beiranvand@modares.ac.ir

**Article Info**

**Article type:**
Research Article

**Article history:**
Received: 23-August-2024
Received in revised form: 17-December-2024
Accepted: 28-December-2024
Published online: 23-Sep-2025

**Keywords**:
Capacitive wireless power transfer,
Electric vehicle charger,
Resonant conversion,
Step up/down.

**ABSTRACT**

This article presents a transformer-less bidirectional converter, which is designed with dual resonant frequencies. It supports Electric Vehicle (EV) charging systems, via capacitive coupling wireless power transfer (CCWPT) technique. In addition, its bidirectional power transfer feature can be used to return energy to the stations of the power-wall systems. This converter smoothly operates in both voltage step-up and step-down operation modes, which provides soft switching conditions for all semiconductor switches. The capacitive coupling technique provides robust galvanic isolation between the primary and secondary sides circuits, while the transformer-less design improves its efficiency and reduces its volume and cost, significantly. The proposed converter supports both full-bridge and half-bridge configurations to adapt to diverse power transfer requirements. The cost-effective CCWPT setup enables multi-EV charging from a single station. A prototype of the given converter has been meticulously developed and experimentally validated, demonstrating excellent performance. The converter efficiently converts output power in a wide range from 200 W to 1000 W, accommodates input voltage from 300 to 500 V, and delivers a 400 V output voltage, which is suitable for EV battery charging. It also achieves a maximum efficiency value of 96%, in practice.

**NOMENCLATURE**

| | | | |
|---|---|---|---|
| $C_{relative}$ | Relative cost. | $n$ | Transformer turn-ratio. |
| $C_r$ | Resonant capacitor. | $Q$ | The quality factor of the resonant circuit. |
| $C_{r\_eq}$ | Equivalent resonant capacitor. | $r$ | Intrinsic resistor. |
| $C_o$ | Output capacitor. | $S_N$ | Normalized cumulative maximum power through all switches and diodes. |
| $D$ | Diode component. | $t_{body(on)}$ | Body diode conducting time. |
| $E_{CN}$ | Normalized cumulative energy is stored in all capacitors. | $t_{delay(on)}$ | Power MOSFET delay for turning on. |
| $E_{LN}$ | Normalized cumulative energy is stored in all inductors. | $t_{dis}$ | 2Cdc discharge time from input voltage to 0 V. |
| $F$ | Normalized switching frequency. | $t_{dead}$ | Dead time between gate-source signals. |
| $f_r$ | Resonant frequency. | $t_{ds(on)}$ | Power MOSFET conducting time. |
| $f_s$ | Switching frequency. | $T_s$ | Switching time ($1/f_s$). |
| $G_{v_g}$ | Converter voltage gain transfer function. | $V_{bF}$ | Forward voltage of the MOSFET body diode. |
| $G_{\omega_s}$ | Output voltage sensitivity to the control signal. | $V_{ds}$ | Power MOSFET drain-source voltage. |
| $I_{ds}$ | Power MOSFET drain-source current. | $V_{gs}$ | Power MOSFET gate-source voltage. |
| $I_{gs}$ | Power MOSFET gate-source current. | $Z_{in}$ | Input impedance. |
| $L_m$ | Magnetizing inductor. | $Z_o$ | Output impedance. |
| $L_r$ | Resonant inductor. | | |

## I. Introduction

In recent years, the proliferation of Electric Vehicles (EVs) has underscored the significance of efficient EV charging and power management within the industry [1]. Concurrently, advancements in Power-Wall technology have aimed to enhance energy storage efficiency by storing energy during periods of low demand and releasing it when needed, offering various advantages [2]. Short-distance wireless power transfer (WPT) methods, typically effective over distances of less than one meter, include Inductive Coupling [3] and Capacitive Coupling [4], where the Capacitive Coupling Wireless Power Transfer (CCWPT) method has emerged as a safer, more cost-effective, and reliable alternative to the Inductive Coupling Wireless Power Transfer (ICWPT) [5].

A compact ICWPT charger for EVs has been introduced in [6], while the charger achieves higher efficiency by eliminating the transformer in its converters, its portable two-section design makes it impractical for large-scale charging stations serving multiple EVs. Another study, given in [7], modified the resonant capacitor of an LLC resonant converter to enable CCWPT. While both configurations ,7] [8 maintain structural simplicity, they suffer from inefficiencies.

Converters employed for CCWPT in prior research [9-11], encountered limitations such as increased power loss due to excessive parallel components. For CCWPT-based EV charging applications [12-15] converters integrated within a car's bumper [12] faced some drawbacks, including hard-switching, low switching frequency, and reduced efficiency. Additionally, CCWPT configurations between the floor and the vehicle's underbody [13-15] exhibited inefficiency caused by high return current and increased power loss, particularly under no-load conditions. A bidirectional converter proposed in [16] suffers from incomplete filtering of switching harmonics, leading to transformer overheating and degraded efficiency. Similarly, a CCWPT solution proposed in [17] positions charging plates between the car's floor and the ground. However, under typical scenarios with standard ground clearance, power transfer remains limited, resulting in suboptimal charging rates. Overall, resonant converters with transformers provide galvanic isolation and voltage regulation. Nevertheless, operating these converters at frequencies deviating from their resonant frequencies introduces additional harmonics into the transformer, which increases its power dissipation. Moreover, considering the cost-effectiveness and structural simplicity of the CCWPT relative to the ICWPT [4], hybrid WPT or ICWPT solutions are financially unsuitable for large-scale deployment.

Many resonant converters equipped with parallel resonant tank components can operate in both step-up and step-down operation modes. However, bidirectional converters are essential for applications such as Power-Wall systems. A previous study introduced a bidirectional resonant converter, but during reverse conduction, switching harmonics are inadequately filtered, resulting in higher power losses. While subsequent studies [19 ,18] attempted to resolve these issues, the incorporation of a transformer led to additional costs, energy losses, and high volume. Although another research work [18], which proposes a three-level bidirectional CLLC converter with a wide input voltage range, has been designed to enhance voltage regulation, it exhibits significant efficiency drops under light-load conditions, alongside higher losses due to the employed transformer, similar to [20]. Furthermore, the present paper provides a comprehensive structure with experimental validation and deeper mathematical analysis.

In [21] and [22], transformer-less converters have been introduced. Although these converters feature a low component count, they experience hard-switching events, causing higher electromagnetic noise and switching power losses. While such issues are not critical at low power levels, they become significant in high-power EV applications, directly affecting efficiency and limiting the converter's suitability for high-power industries. In [23], an EV charger has been proposed; however, the lack of empirical evidence and detailed mathematical analysis limits further investigation. The converter also needs a broad switching frequency range and lacks constant current control. Similarly, in [24], a DC-DC converter has been introduced with persisting issues of noise and incomplete soft-switching operation. Other research works in [25, 26] introduce some converters that lack adequate filtering before the transformer, allowing harmonics to pass through the transformer and cause heating, which ultimately restricts power density. Some other converters for EV charging with soft-switching operation are proposed in [27-29], but their employed transformers increase their sizes, cost, and power losses. These converters operate at wide switching frequency ranges, which reduce their efficiencies and result in significant circulating currents under off-resonant conditions. In terms of multi-output charging, most of these converters incorporated transformers, which, while supporting high-power applications, escalated costs and posed control challenges under varying load conditions. In [30] multi-output transformers faced similar drawbacks, including a high number of components. The problem of input/output isolation, as well as broad switching frequency ranges, persisted in [31-33], complicating control over a wide power range.

This paper introduces a bidirectional transformer-less isolated resonant converter, which can be designed specifically for CCWPT applications. Using the CCWPT

technique not only reduces costs but also enables the charger to accommodate multiple vehicles simultaneously. The transformer-less architecture contributes to enhancing efficiency and reducing the weight, while capacitive coupling ensures reliable input-output isolation. The optimally designed resonant tank mitigates harmonics in both forward and backward power flow operation modes. The bidirectional capability further supports Power-Wall applications, enabling flexible battery allocation. Additionally, the CCWPT inherently provides robust isolation between the input and the output ports. To limit frequency variations, a combination of the half-bridge and the full-bridge topologies has been adopted, which minimizes the frequency deviations and enhances the efficiency, in practice.

The proposed converter and its key waveforms are given in Section II, and then its mathematical analysis is given in Section III. Next, a design procedure is introduced in Section IV, in detail. The proposed converter experimental results are described in Section V. Finally, the paper is concluded in Section.

## II. Proposed Converter and Its Key Waveforms

The proposed converter, shown in Fig. 1, is a novel transformer-less bidirectional resonant converter tailored specifically for Capacitive Coupling Wireless Power Transfer (CCWPT) applications. By reconfiguring the resonant capacitors into two series connections, the design achieves effective isolation between the input and output ports, eliminating the need for a transformer. This architecture is optimized for wireless power transfer (WPT) applications, with the primary side of the resonant capacitors installed on a wall structure and the secondary side embedded within the EV's bumper. Fig. 2 illustrates the key waveforms of the converter, highlighting essential operational characteristics and performance metrics. These waveforms include critical parameters such as input voltage, input current, output voltage, output current, and switching signals, offering a comprehensive view of the converter's behavior across varying operating conditions. Fig. 3 demonstrates a typical EV charging scenario, displaying the converter's practical application in real-world conditions. In this setup, capacitive plates are strategically positioned on both the wall and the car's bumper, separated by a dielectric foam layer. As the EV approaches the wall, the plates align, with the dielectric layer preventing any short circuits. With a separation distance of around 1 mm, it is possible to achieve capacitance values in the Nano Farad (*nF*) range. The foam layer on the wall side provides flexibility, ensuring reliable and consistent contact between the plates. A notable advantage of the proposed design is that all key components are housed on the wall side, resulting in a lighter and more compact setup on the vehicle. This centralized configuration enhances cost-effectiveness by allowing the wall-side infrastructure to be universally applied to multiple vehicles, making it more economical than designs with components embedded within each vehicle. While a hybrid WPT setup with an inductor on the vehicle side is considered, the use of the car's bumper for CCWPT requires an alternative approach to inductive coupling. Given the diversity of vehicles that may adopt this technology, extensive inductive windings on each vehicle would be cost-prohibitive.

In summary, the proposed converter offers a transformer-less, cost-effective solution for efficient CCWPT in EV charging applications. Its design ensures robust input-output isolation and demonstrates the feasibility and practicality of implementing the CCWPT through capacitive coupling techniques.

## III. Mathematical Analysis

Text Both First Harmonic Approximation (FHA) and small signal models of the converter, as well as its different components power losses, are given here, respectively.

### *A. FHA model*

To enable a streamlined yet effective analysis of the proposed converter, the FHA method is applied, which is solely focused on the first harmonics of the different switching waveforms of the converter, while omitting higher-order harmonics, as detailed in [33].

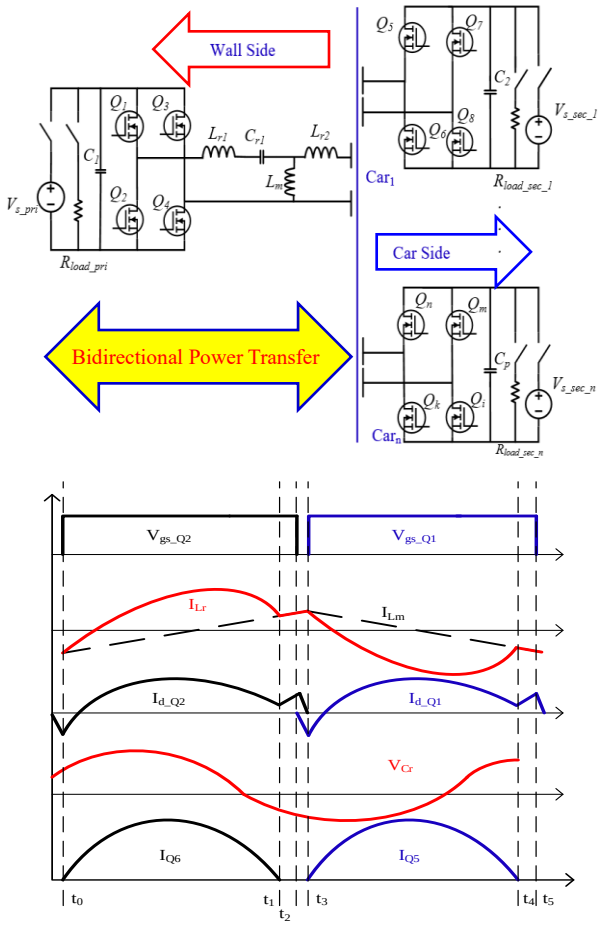


Fig. 1. Key waveforms of the proposed converter.

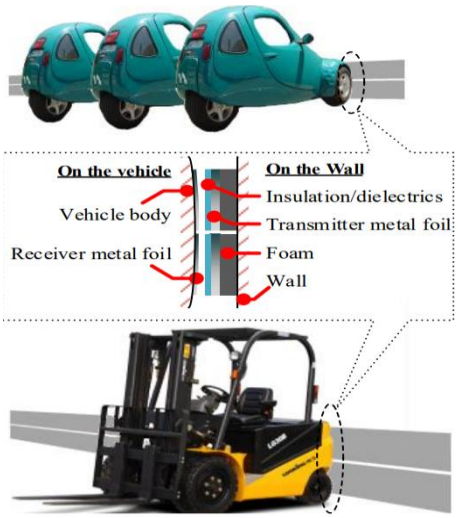


Fig. 3. A typical application of the proposed converter.

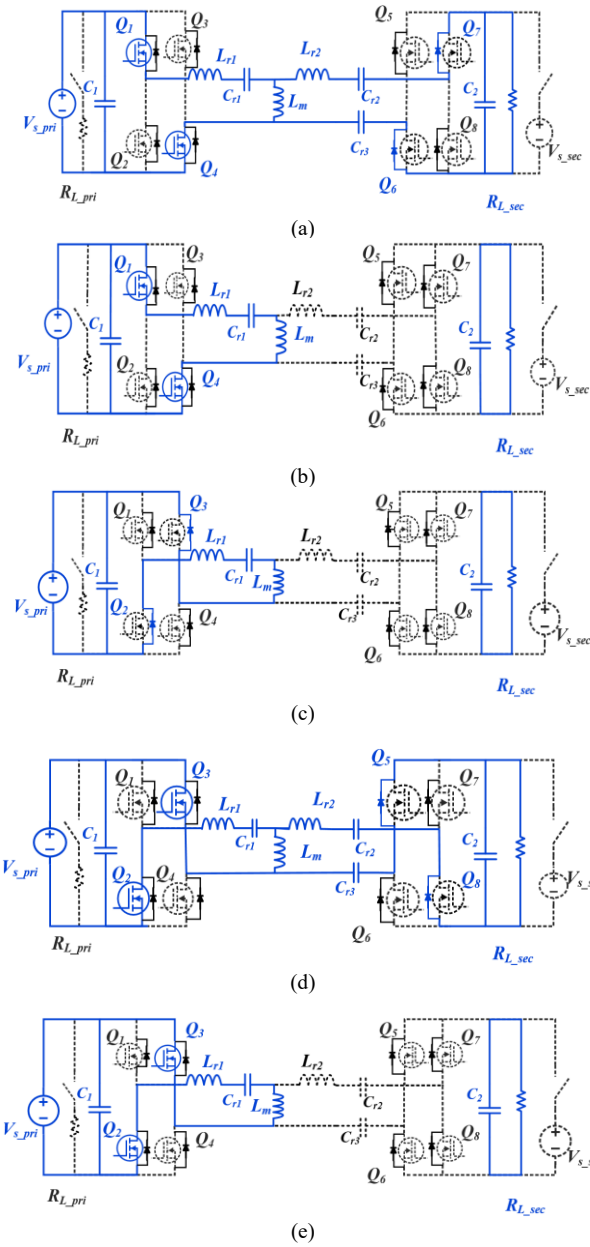


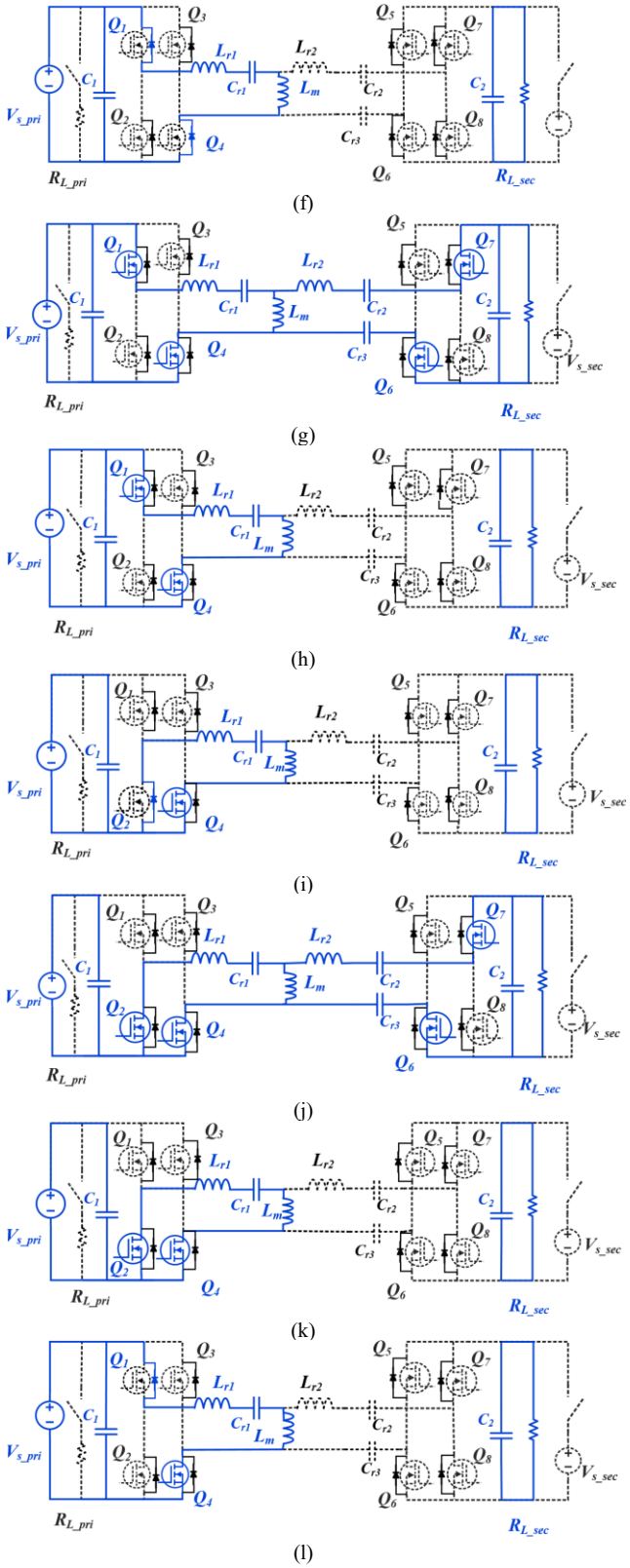


Fig. 4. Different operational states of the proposed converter in forward operation mode, (a)-(f) full-bridge configuration, and (g)-(l) half-bridge configuration.

Using the FHA approach, equivalent circuits of the converter are derived, creating a simplified framework for evaluating the converter's performance and core

characteristics. Fig. 5(a) shows the equivalent circuit of the proposed converter based on the FHA method, which reduces the complexity of the overall structure by focusing exclusively on the first harmonic components. This simplification enhances understanding and analysis of the converter's behavior. Additionally, Fig. 5(b) provides a more condensed representation of the FHA-based equivalent circuit, aiding in mathematical analysis and extraction of key converter parameters. The following equations describe the relationships between various parameters within the FHA framework:

$$\begin{cases} i_{L1}(t) = C_{r3}\dfrac{d}{dt}v_{c3}(t), \\ i_{L2}(t) = C_{r_{eq}}\dfrac{d}{dt}v_{ce}(t), \\ i_{Lm}(t) = i_{L1}(t) - i_{L2}(t). \end{cases} \quad (1)$$

$$C_{r_{eq}} = \frac{C_{r1}C_{r2}}{C_{r1}+C_{r2}}, R_{eq} = \frac{8}{\pi^2}R_L, F = \frac{f_s}{f_r}, \quad m = 1 + \frac{L_m}{L_r}. \quad (2)$$

$$\begin{cases} V_1 = \dfrac{2V_{in}}{\pi} sin(2\pi f_s t) \ \ For\ Full\ bridge, \\ V_1 = \dfrac{V_{in}}{\pi}\sin(2\pi f_s t) \ \ For\ Half\ bridge. \end{cases} \quad (3)$$

$$Q = \frac{\sqrt{L_r/C_r}}{R_e}, C_r = \frac{1}{2\pi f_s R_e Q}, L_r = \frac{1}{(2\pi f_s)^2 C_r}. \quad (4)$$

$$f_{r1} = \frac{1}{2\pi\sqrt{L_{r1}C_{r1}}}, \quad f_{r2} = \frac{1}{2\pi\sqrt{(L_{r1}+L_m)C_{r1}}}. \quad (5)$$

The first harmonic approximation strikes a balance between accuracy and complexity reduction in the analysis. Considering the given simplified equivalent circuit of the proposed converter, as shown in Fig. 5(b), we can write:

$$v_1(t) - v_{Lr1}(t) - v_{Lm}(t) - v_{c1}(t) = 0 \quad (6)$$

$$v_2(t) - v_{Lr2}(t) - v_{Lm}(t) - v_{ce}(t) = 0 \quad (7)$$

Here, $Q$ represents the converter quality factor, $F$ is the normalized switching frequency, and $f_s$ is the switching frequency. Additionally, $f_{r1}$ and $f_{r2}$ denote the converter's first and second resonant frequencies, respectively. $n$ also denotes the transformer turn ratio. The converter's voltage gain is derived through straightforward algebraic calculations as follows:

$$\frac{V_o}{V_{in}} = \frac{(m-1)F^2}{n\sqrt{(F^2m-1)^2 + F^2(F-1)^2(m-1)Q^2}}. \quad (8)$$

Fig. 6 shows the proposed converter voltage gain versus the normalized switching frequency in full- and half-bridge configurations, by considering (8) under different conditions.

### B. Small Signal Model

In the resonant converters, absence of the DC current and voltage components across certain circuit elements of the resonant tank can complicate small-signal modeling by using the traditional methods. However, as outlined in [34], if the modulation frequency is significantly lower than the switching frequency, the resonant capacitor can be approximated as an inductor, thereby simplifying the small-signal model of the converter.

Since the proposed converter employs an LLC resonant circuit; its seventh-order model can be reduced to a third-order LLC model. Furthermore, according to [34], this third-order model can be further simplified to a second-order model, as depicted in Fig. 7, with the relevant equations derived in (9) to (15) in this section.

The frequency response of this small-signal model is shown in Fig. 8(a). To regulate the output voltage under step input voltage and load changes, a conventional Proportional-Integral (PI) controller is employed, where its frequency response is plotted in Fig. 8(b). The closed-loop system frequency response is also given in Fig. 8(c), while Fig. 8(d) shows the time-domain response of the closed-loop configuration, demonstrating robust performance under input and output disturbances. The converter with its control scheme is illustrated in Fig. 8(e), too. For simplicity, the forward conduction mode is depicted, here; however, the converter operates similarly during backward conduction mode. A microcontroller (μC) is utilized as a voltage-controlled oscillator (VCO) to implement the conventional pulse-frequency modulation (PFM) technique. The microcontroller dynamically determines whether the converter operates in its half-bridge or full-bridge operation mode depending on the output power and input voltage conditions.

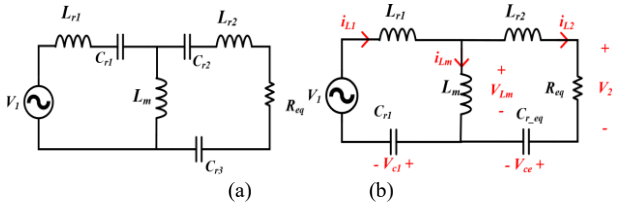


Fig. 5. (a) FHA equivalent circuit of the proposed converter and (b) its simplified equivalent circuit.

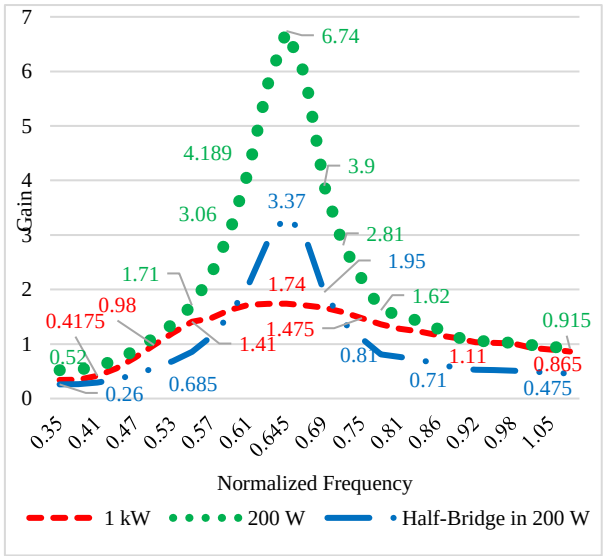


Fig. 6. Voltage gain of the proposed converter versus normalized switching frequency in the full- and half-bridge configuration.

Some key transfer functions and main parameters of the proposed converter are summarized, here, as follows:

$$G_{\omega_s}(s)=\frac{\hat{V}_o(s)}{\hat{\omega}_s(s)}=\frac{G_{DC}\left(X_{eq}^2+R_{eq}^2\right)}{\left(s^2L_e^2+sL_eR_{eq}+X_{eq}^2\right)}\times\frac{1}{\left(1+R_LC_fs\right)+R_{eq}\left(sL_e+R_{eq}\right)} \quad (9)$$

$$G_{DC}=\frac{V_g}{2n}\frac{L_n}{\omega_o\omega_n}\times\frac{\left(\frac{1}{\omega_n^2}-\omega_n^2\right)\left(\frac{\pi^2}{8}QL_n\right)^2-\left(L_n+1-\frac{1}{\omega_n^2}\right)\left(\frac{2}{\omega_n^2}\right)}{\left(\sqrt{\left(L_n+1-\frac{1}{\omega_n^2}\right)^2+\left(\left(\frac{1}{\omega_n}-\omega_n\right)\frac{\pi^2}{8}QL_n\right)^2}\right)^3} \quad (10)$$

$$L_e=\left(1+\frac{\Omega_o^2}{\Omega_s^2}\right)L_r,\ X_{eq}=\Omega_sL_r-\frac{1}{\Omega_sC_r},\ L_n=\frac{L_m}{L_r} \quad (11)$$

$$G_{v_g}(s)=\frac{\hat{V}_o(s)}{\hat{V}_g(s)}=\frac{M_{st}}{2n}\times\frac{R_{eq}^2+X_{eq}^2+L_eR_{eq}s}{\left(s^2L_e^2+sL_eR_{eq}+X_{eq}^2\right)}\times\frac{1}{\left(1+R_LC_fs\right)+R_{eq}\left(sL_e+R_{eq}\right)} \quad (12)$$

$$M_{st}=\left\|\frac{j\omega_nL_n}{j\omega_n\left(L_n+1-\frac{1}{\omega_n^2}\right)+\frac{\pi^2}{8}Q(1-\omega_n^2)L_n}\right\| \quad (13)$$

$$Z_o(s)=\frac{R_L\left(s^2L_e^2+X_{eq}^2+sL_eR_{eq}\right)}{\left(s^2L_e^2+sL_eR_{eq}+X_{eq}^2\right)}\times\frac{1}{\left(1+R_LC_fs\right)+R_{eq}\left(sL_e+R_{eq}\right)} \quad (14)$$

$$Z_{in}(s)=\frac{\pi^2}{2}\times\frac{\left(s^2L_e^2+sL_eR_{eq}+X_{eq}^2\right)}{s^2L_eC_fR_L+sL_e+sX_fR_L\frac{R_{eq}^3}{R_{eq}^2+X_{eq}^2}+R_{eq}}\times\left(1+R_LC_fs\right)+R_{eq}\left(sL_e+R_{eq}\right) \quad (15)$$

## C. Power Losses Analysis

Here, power losses of the different components of the proposed converter are given, in summary.

### 1. Diode Power Loss

$$i_{D1}(t)=\begin{cases}nI_{Rm}\sin(\omega_rt), & 0\le t<\frac{1}{2}T_o\\ 0. & \frac{1}{2}T_o\le t<T_s\end{cases} \quad (16)$$

$$i_{D2}(t)=\begin{cases}0, & 0\le t<\frac{1}{2}T_s\\ nI_{Rm}\sin(\omega_rt), & \frac{T_s}{2}\le t<\frac{T_s+T_0}{2}\\ 0. & \frac{T_s+T_0}{2}\le t<T_s\end{cases} \quad (17)$$

Where, $\omega_r=2\pi f_r$. The average and RMS current values of each diode are respectively equal to:

$$I_{D1avg}=\frac{I_o}{2}=\frac{\pi I_o}{4}\sqrt{\frac{f_r}{f_s}},\quad I_{RMS}=\frac{\pi I_o}{2n\frac{f_s}{f_r}} \quad (18)$$

Power losses due to the forward voltage drop, $V_f$, and conduction resistance, $r_f$, of each diode are respectively equal to:

$$P_{Vf}=V_fI_{D1avg}=V_f\frac{I_o}{2}=\frac{V_f}{V_o}\frac{P_o}{2} \quad (19)$$

$$P_{rf}=I_{D1rms}^2r_f=\frac{\pi^2}{16}\frac{f_r}{f_s}\frac{r_f}{R_L}P_o \quad (20)$$

Therefore, each diode's total conduction loss is identified, easily.

$$P_D=P_{D1}+P_{D2}=\left(\frac{V_f}{V_o}+\frac{\pi^2}{8}\frac{f_r}{f_s}\frac{r_F}{R_L}\right)P_o \quad (21)$$

### 2. Output Capacitor Power Loss

Output capacitor current can be identified as follows:

$$I_{Co}(t)=\begin{cases}nI_{Rm}\sin(2\omega_rt)-I_o, & 0\le t<\frac{T_0}{2}\\ -I_o. & \frac{T_0}{2}\le t<T_s\end{cases} \quad (22)$$

$$I_{Co\_rms}=I_o\sqrt{\frac{\pi^2}{8}\frac{f_r}{f_s}-1} \quad (23)$$

Therefore, its power loss is given as follows:

$$P_{r_{Co}}=I_{Co_{rms}}^2r_{Co}=\left(\frac{\pi^2}{8}\frac{f_r}{f_s}-1\right)I_o^2r_{Co}=\left(\frac{\pi^2}{8}\frac{f_r}{f_s}-1\right)\frac{r_{Co}}{R_L}P_o \quad (24)$$

In addition, the following parameters are defined here to calculate each MOSFET total power loss.

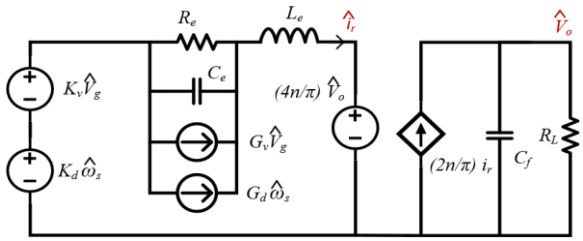


Fig. 7. Small-signal model of the proposed converter.

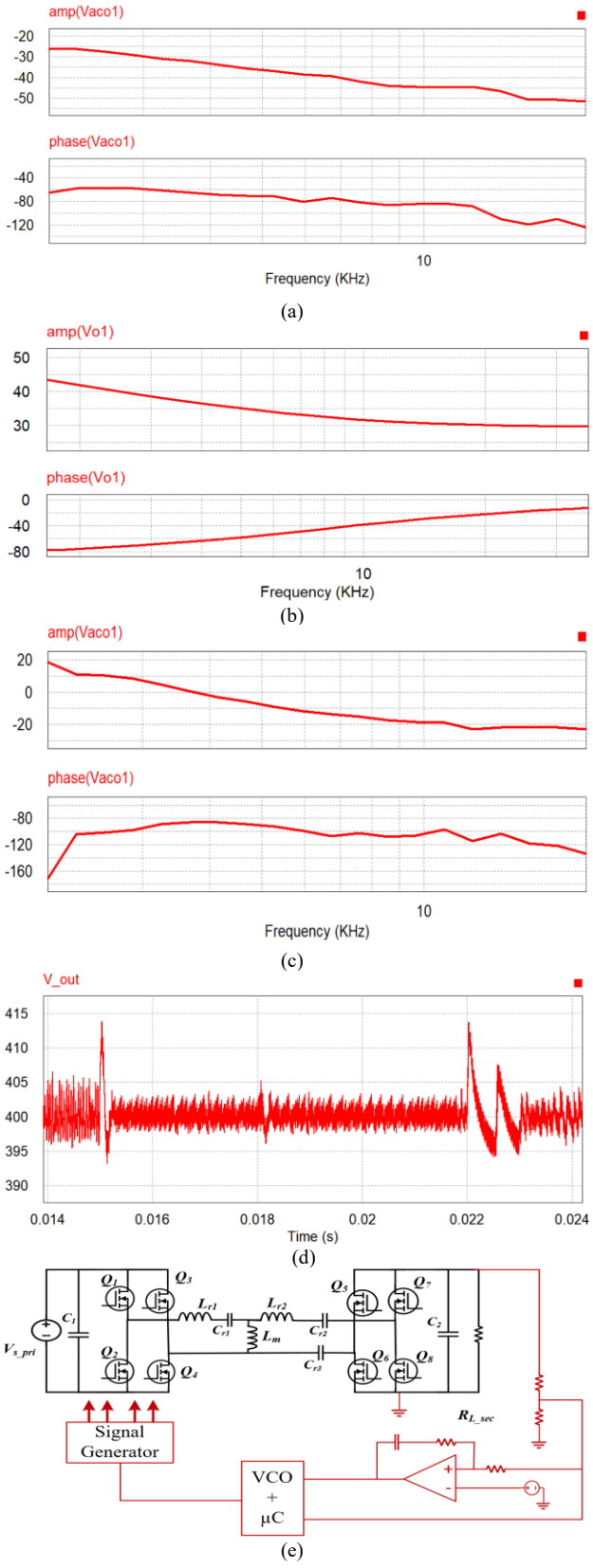


Fig. 8. Bode diagrams of proposed converter (a) without compensation, (b) PI-controller designed for the converter, (c) closed loop structure of the proposed converter, (d) simulated output voltage of the proposed converter under load and input voltage step variations, and (e) proposed converter and its control circuit in one operation mode.

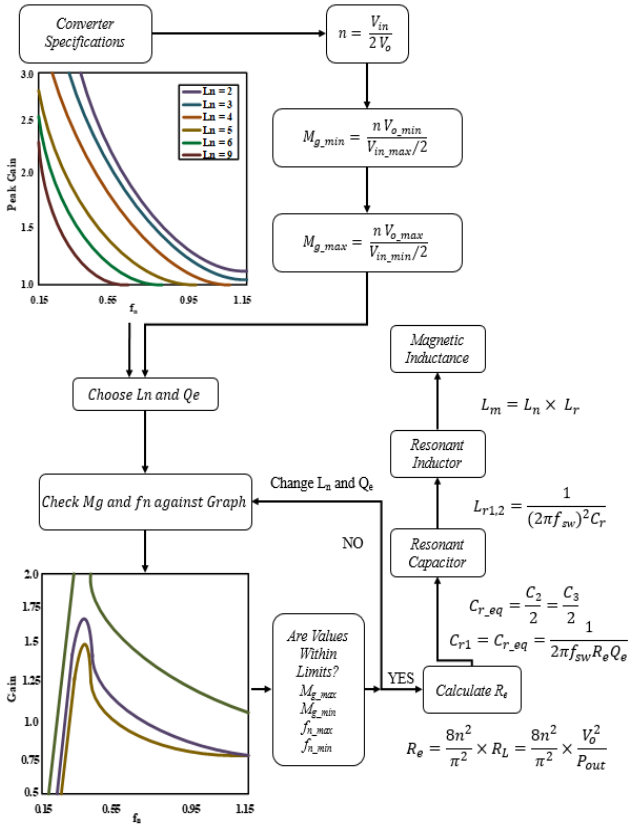


Fig. 9. Design procedure of the proposed converter.

$t_{dis}$: $2C_{dc}$ discharge time from input voltage to 0 V.
$t_{dead}$: dead-time between gate-source signals.
$t_{delay(on)}$: power MOSFET turning on the delay time.
$t_{body(on)}$: body diode conducting time.
$V_{gs}$: power MOSFET gate-source voltage.
$V_{bF}$: power MOSFET body diode forward voltage.
$t_{ds(on)}$: power MOSFET conducting time.

### 3. Driving MOSFET Power Loss

This loss is due to gate-source power MOSFET capacitor charge and discharge, which is given as follows:

$$P_{drive} = 2\left(\frac{1}{2} C_{gs} V_{gs}^2\right) f_s \tag{25}$$

### 4. Power Loss of Body Diode of Each Power MOSFET

$$t_{dis} = \frac{8}{M_g} L_m (C_{ds1} + C_{ds2}) f_s \tag{26}$$

$$t_{body(on)} = t_{dead} - t_{dis} + t_{delay(on)} \tag{27}$$

$$P_{body} = 2V_{bF}\left[\left(\frac{n.V_o}{L_m}\left(\frac{1}{4}\frac{1}{f_s} - t_{dis}\right)\right)\right] t_{body(on)}.f_s \tag{28}$$

### 5. Power MOSFETs Turning off Power Loss

Two assumptions are made, here: the first one is in the meanwhile of power MOSFET turning off, the power MOSFET current is near the magnetizing inductor current. The second one is rising voltage and the magnetizing inductor current is linear.

$$V_{ds}(t) = V_{ds(on)} + \frac{V_{in} - V_{ds(on)}}{t_{dis}} t \tag{29}$$

$$i_{ds}(t) = \frac{nV_o}{L_m}\frac{1}{4f_s}\left(1 - \frac{t}{t_{dis}}\right) \quad (30)$$

$$p_{tf} = 2f_s \int_0^{t_{dis}} v_{ds}(t) i_{ds}(t) dt = \frac{nV_o t_{dis}\left(V_{in} + 2V_{ds(on)}\right)}{12L_m} \quad (31)$$

*6. Body Diode MOSFET Power Loss*

$$t_{dis} = \frac{8}{M_g} L_m (C_{ds1} + C_{ds2}) f_s \quad (32)$$

$$t_{body(on)} = t_{dead} - t_{dis} + t_{delay(on)} \quad (33)$$

$$P_{body} = 2V_{bF}\left[\left(\frac{n.V_o}{L_m}\left(\frac{1}{4}\frac{1}{f_s} - t_{dis}\right)\right)\right] t_{body(on)}.f_s \quad (34)$$

TABLE I Main Specifications of the Proposed Converter Prototype.

| Parameter | Value |
|---|---|
| Input Voltage | 300-500 *V* |
| Output Voltage | 400 *V* (suitable for EV charging) |
| Switches | N60E23 |
| Microcontroller | STM32F103 |
| Gate-Drive | TC4427 |
| Switching Frequency | 470-715 *kHz* |
| Output Power | 200-1000 *W* |
| $C_1$ , $C_2$ | 2×10 *nF* |
| $C_3$ | 5 *nF* |
| $L_{r1}$ , $L_{r2}$ | 2×10 *μH* |
| $L_m$ | 14 *μH* |
| $C_{out}$ | 5 *μF* |

## IV. Design procedure

A design procedure is given here for the proposed converter to determine the optimal values of its key components to achieve the desired performance and operational characteristics. The symmetrical configuration of the proposed converter simplifies its design procedure and improves overall efficiency. Specifically, the capacitance values are chosen to establish a symmetrical structure, such that $C_{r2}=C_{r3}=2C_{r1}=2C_{r\_eq}$, and the inductance values are selected to ensure symmetry, with $L_{r1}=L_{r2}$. By adopting this symmetrical structure, the converter can be analyzed as an LLC resonant structure, where the resonant frequencies $f_{r1}$ and $f_{r3}$ are equal:

$$f_{r1} = \frac{1}{2\pi\sqrt{L_{r1}C_{r1}}} = f_{r3} = \frac{1}{2\pi\sqrt{L_{r2}C_{r_{eq}}}} \approx f_s \quad (35)$$

These resonant frequencies are two critical design parameters, which significantly affect the converter performance. The selection of capacitance and inductance values is based on achieving the desired resonant frequencies, which are determined by considering input and output voltage requirements, power ratings, and efficiency targets. These factors influence the choice of switches, capacitors, and inductors. Furthermore, the design methodology incorporates considerations beyond electrical specifications, such as physical layout optimization, effective thermal management, and mitigation of electromagnetic interference (EMI). This comprehensive approach aims to enhance various aspects of the converter's performance, including efficiency, compactness, cost-effectiveness, and reliability. Throughout the design phase, simulation tools, and rigorous mathematical analyses are utilized to validate the system's performance and fine-tune component values for optimal results.

The different design steps for the proposed converter are outlined in summary as follows:

*Step (I) Determine the Input and Output Voltages Variation Ranges:* Establish the maximum and minimum values of the input and output voltages based on the design specifications.

*Step (II) Calculate Transformer Turns Ratio (n):* Use the given input and output voltage values to calculate the required transformer turns ratio.

*Step (III) Set Voltage Gain Boundaries:* Determine the minimum and maximum voltage gain boundaries based on the design requirements and constraints.

*Step (IV) Determine Quality Factor (Q) and Inductance Ratio ($L_n$):* Calculate the necessary $Q$-factor and inductance ratio ($L_n$) using the gain-frequency characteristics of the LLC resonant converter.

*Step (V) Calculate Resonant Tank Component Values:* Using (4) and (5), calculate the values of the resonant tank components (i.e., $L_r$, $L_m$, and $C_{r\_eq}$) to ensure optimal performance.

The overall design procedure is summarized in Fig. 9, which provides a visual representation of the systematic design process for the proposed converter.

## V. Experimental Results

The proposed transformer-less bidirectional converter underwent a thorough experimental evaluation, combining simulation analyses with practical testing. Tailored for applications such as EV charging and Power-Wall energy storage, the converter leverages CCWPT technology to enable both step-up and step-down operation modes.

It functions efficiently between two defined resonant frequencies, ensuring seamless transitions between these operating modes. When the switching frequency surpasses the upper limit, the converter intuitively transitions from a full-bridge to a half-bridge configuration. A prototype converter, as shown in Fig. 10 and specified in Table I, is implemented and subjected to comprehensive testing under extreme conditions to validate its performance. Experimental results, detailed in Figs. 11 and 12, highlight

the converter's reliable functionality even under demanding scenarios.

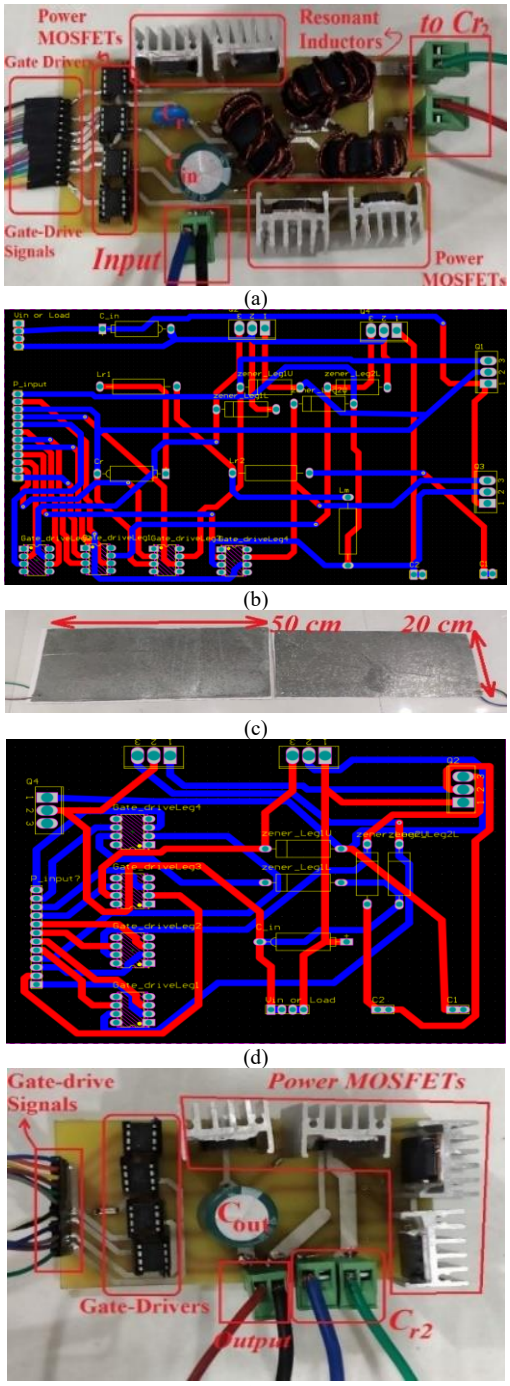


(a) (b) (c) (d) (e)

Fig. 10. Prototype of the proposed converter (a) primary section, (b) PCB of the primary section, (c) capacitors for the CCWPT part, (d) PCB of the secondary section, and (e) secondary part of the prototype converter.

The recorded waveforms from testing substantiate the system's ability to maintain stable and efficient operation across its range of applications. A detailed comparison of the proposed transformer-less bidirectional resonant converter with other EV chargers in the literature is tabulated in Table II and illustrated in Fig. 13. This analysis evaluates key performance metrics, including efficiency, operational complexity, size, cost, and reliability. Using [5], (36), and (37), this comparison highlights several distinct advantages of the proposed converter over the existing solutions, as follows for the papers in Table II:

$$\begin{cases} E_{LN} = \dfrac{\left(\frac{1}{2}L_r I_{Lr}^2\right)}{P_{max}T_s}, \\ E_{CN} = \dfrac{\frac{1}{2}C_r V_{Lr}^2}{P_{max}T_s}, \\ S_N = \dfrac{1}{P_{max}}(V_{max\,S}I_{max\,S} + V_{max\,D}I_{max\,D}). \end{cases} \tag{36}$$

$$\begin{cases} C_{relativve} = \\ \dfrac{n}{P_{max}}(3(V_{max\,S}I_{max\,S}) + V_{max\,D}I_{max\,D}) \\ n = 1 \rightarrow LOW\ \ nom.of\ Components, \\ n = 1.25 \rightarrow MED.\ nom.of\ Components, \\ n = 1.5 \rightarrow HIGH\ \ nom.of\ Components. \end{cases} \tag{37}$$

1) The bulky transformer is not used in the transformer-less architecture, which significantly reduces its size, weight, and cost as compared to the traditional transformer-based topologies [27-29, 34-37]. This reduction in physical component count not only reduces the manufacturing and maintenance costs, but also improves the power density.
2) The proposed methods use the CCWPT to ensure robust isolation between the input and output ports without requiring a magnetic transformer, simplifying the overall design and reducing electromagnetic interference (EMI).
3) The proposed converter's high efficiency is another critical advantage in comparison to [7, 12, 27, 34, 35]. Experimental validation, as shown in Fig. 14, demonstrates a maximum efficiency of up to 96%, outperforming most other solutions listed in Table II. This high efficiency is achieved through the implementation of soft-switching techniques, such as ZVS and ZCS.
4) The converter ZVS and ZCS soft-switching operations minimize the EMI noise and power switching losses that make it possible to design the converter at high switching frequencies. High-frequency operation reduces volumes of the passive components including the required filters and resonant tank components, achieving a more compact, efficient, high power density, and reliable structure, in practice. These features not only improve energy conversion performance but also reduce thermal stress on the components, extending their operational lifespan, too.
5) Furthermore, the flexibility of the proposed converter stands out in its ability to seamlessly transition between half-bridge and full-bridge configurations, which enables the converter to operate efficiently in both step-up and step-down operation modes, maintaining consistent performance across a wide range of input and output voltage conditions contrary to converters in [7, 12]. In contrast, many conventional chargers are limited to either step-up or

step-down operation, which restricts their application scope such as converters in [27-29, 34-37].

6) The ability to adapt the switching frequency within a controlled range further minimizes switching stress, enhancing reliability and operational stability.
7) Reliability and safety are other advantages of the proposed method. The converter incorporates an overload protection mechanism, which defines a safe power margin and employs current protection to prevent damage under fault conditions. This feature, combined with the compact and simplified design, ensures dependable performance even under the worst-case scenarios.

Table II demonstrates that the proposed converter outperforms others in terms of operational simplicity and robustness, making it a more viable option for practical applications. In summary, the proposed transformer-less bidirectional resonant converter offers several benefits over the other existing methods, including superior efficiency, compactness, operational flexibility, and reliability. These attributes, as highlighted in Table II and supported by experimental results, establish the proposed solution as a cutting-edge alternative for EV charging and Power-Wall applications, addressing the limitations of current technologies while meeting the demands of modern power conversion systems.

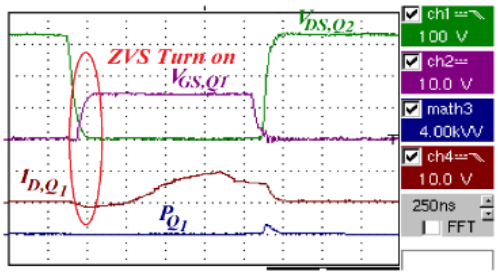


(a)

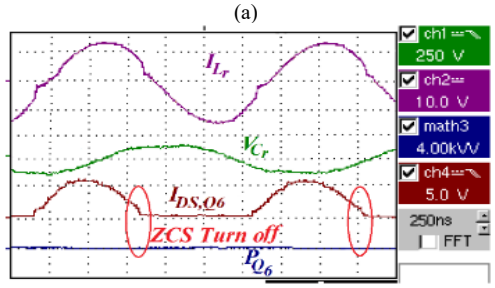


(b)

Fig. 11. Experimental open-loop waveforms of the proposed converter at 300 V input voltage and 1 kW output power: (a) gate-source voltage of $Q_1$, drain-source voltage of $Q_2$, and drain current and loss of $Q_1$, respectively, and (b) Current through $L_r$, voltage across $C_r$, and current and loss of $Q_6$, respectively.

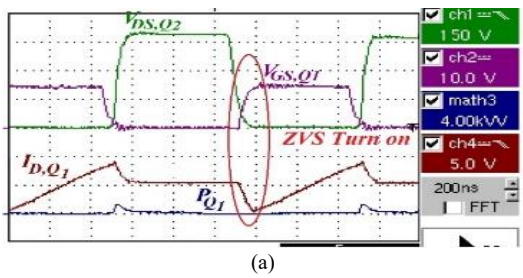


(a)

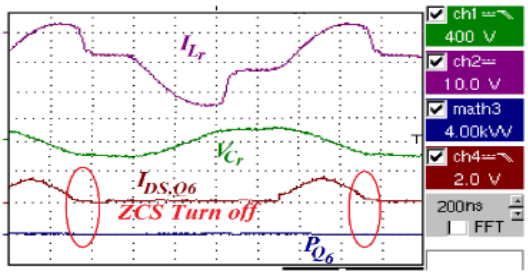


(b)

Fig. 12. Experimental open-loop waveforms of the proposed converter under 500 V input voltage and also 200 W output power values, (a) gate-source voltages of $Q_1$ and drain-source of $Q_2$, $Q_1$ drain current and loss, respectively, and (b) $L_r$ current, $C_r$ voltage, $Q_6$ current and its loss, respectively.

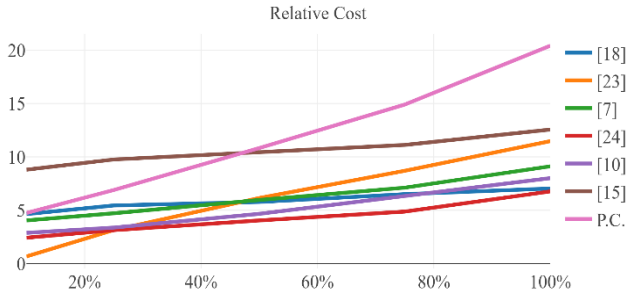


*P.C.: Proposed Converter

(a)

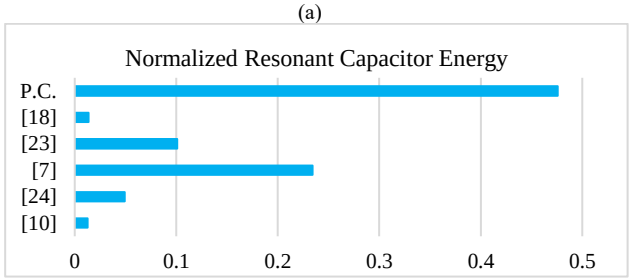


(b)

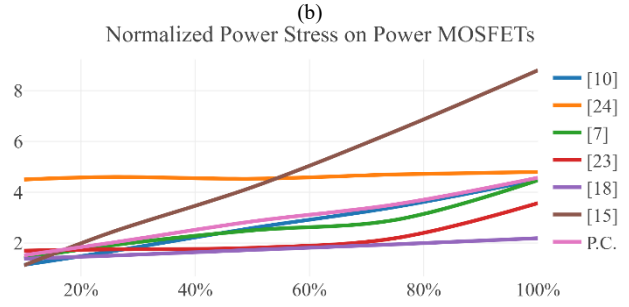


(c)

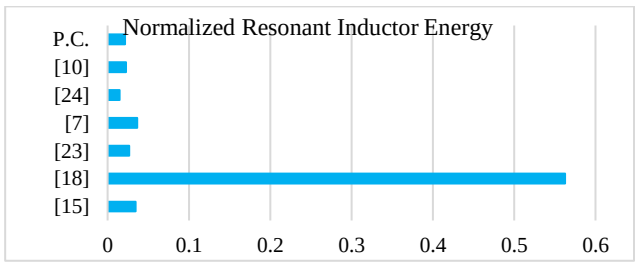


(d)

Fig. 13. Comparison of the proposed converter (P.C.) with some conventional converters including a comparison of (a) relative cost, (b) normalized resonant capacitor energy (c) normalized power stress on power MOSFETs, and (d) normalized resonant inductor energy.

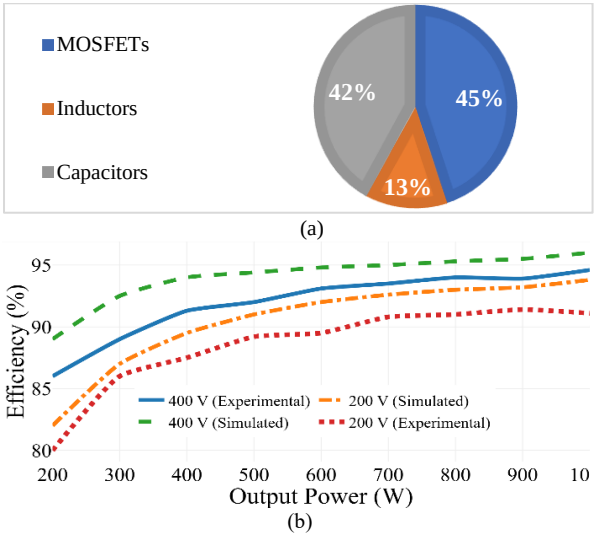


Fig. 14. (a) Power losses of the MOSFETs, inductors, and capacitors used in the prototyped converter and (b) simulated and experimental efficiency curves of the proposed converter versus output power.

## VI. Conclusion

This paper proposes a novel transformer-less bidirectional resonant converter utilizing the CCWPT technique for EV charging and Power-Wall applications. By eliminating the transformer and employing capacitive coupling, the design achieves robust input-output port isolation, a maximum efficiency of 96%, reduced volume, weight, and cost, as well as high power density—addressing critical challenges in modern power conversion systems. The bidirectional functionality enables seamless integration with Power-Wall systems, supporting partial allocation of EV battery storage. The converter's ZVS and ZCS soft-switching operations, experimentally validated, minimize EMI noise and switching losses, allowing for high-frequency operation. This reduces the volume of passive components, including filters and resonant tank elements, resulting in a compact, efficient, high-power-density, and reliable design. Additionally, the converter generates sinusoidal current and voltage waveforms with low harmonic distortion, ensuring efficient power transfer across capacitive plates and magnetic components. The ability to transition between half-bridge and full-bridge configurations reduces the switching frequency range, facilitating both step-up and step-down operations with minimal switching stress. Experimental results underscore the converter's potential as an efficient and practical solution for wireless EV charging and energy storage systems, advancing the state of power electronics research.

TABLE II Comparison of the Proposed Converter with Conventional Resonant Converters

| Application | Reference | Input voltage (V) | Output voltage (V) | Output power (W) | Maximum Efficiency (%) | Switching frequency (kHz) | $L_r$ (µH) | $C_r$ (nF) | $L_m$ (µH) | Control complexity | Number of components |
|---|---|---|---|---|---|---|---|---|---|---|---|
| EV Charger | [34] | 100 | 100 | 200 | 92 | NM* | 41 | 120 | NM | Low | 15 |
| | [35] | 400 | 50-450 | 300 | 94 | 32-100 | 34 | 70 | 108 | Low | 19 |
| | [29] | 350-400 | 200-700 | 1000 | 96 | 65-150 | 21 | 94 | 140 | Low | 14 |
| | [28] | 540 | 120 | 1500 | 96 | 100 | 9 | 2.5 | 17 | Low | 20 |
| | [27] | 400 | 670-800 | 2000 | 91 | 75-130 | 35.2 | 71 | 105.6 | Low | 18 |
| | [36] | 120 | 0-80 | 600 | 96 | 140 | 30 | 60 | 45 | Medium | 12 |
| | [37] | 400 | 150-450 | 3300 | 96.9 | 150-250 | 18.4 | 22 | 2× 50 | Low | 20 |
| ICWPT | [7] | 100 | 24 | 33 | 95 | 100 | 800 | 3 | 12000 | Low | 14 |
| CCWPT | [12] | 240 | 185 | 1000 | 92 | 1000 | NM | 10 | NM | Medium | 12 |
| | The proposed Converter | 300-500 | 400 | 1000 | 96 | 470-720 | 10 | 5 | 13 | Low | 17 |

* Not Mentioned

## REFERENCES


[1] M. Eberhard and M. Tarpenning, "The 21 st century electric car tesla motors," *Tesla Motors*, vol. 17, 2006.

[2] P. Bulman, "Tesla's Powerwall battery production requires 'super-charged'supply chain," *Renewable Energy Focus*, vol. 16, no. 5-6, pp. 126-127, 2015.

[3] Y. Zhang, S. Chen, X. Li, and Y. Tang, "Design of high-power static wireless power transfer via magnetic induction: An overview," *CPSS Transactions on Power Electronics and Applications*, vol. 6, no. 4, pp. 281-297, 2021, doi: 10.24295/CPSSTPEA.2021.00027.

[4] F. Lu, H. Zhang, and C. Mi, "A review on the recent development of capacitive wireless power transfer technology," *Energies*, vol. 10, no. 11, p. 1752, 2017, doi: 10.3390/en10111752.

[5] J. Shahsevani and R. Beiranvand, "An Application-Oriented Review of the LLC-Based Resonant Converters," *IEEE Access*, 2024, doi: 10.1109/ACCESS.2024.3386430..

[6] J. Shahsevani and R. Beiranvand, "A Compact, High Efficiency, and Portable Wireless EV Resonant Charger," *International Journal of Industrial Electronics Control and Optimization*, 2024, doi: 10.22111/ieco.2024.49636.1611.

[7] T. Mohamed, A. Becetti, and S. Bayhan, "Design and analysis of full bridge LLC resonant converter for wireless power transfer applications," pp. 1-5, 2018, doi: 10.1109/CPE.2018.8372606.

[8] D. Rozario, N. A. Azeez, and S. S. Williamson, "A modified resonant converter for wireless capacitive power transfer systems used in battery charging applications," in *2016 IEEE Transportation Electrification Conference and Expo (ITEC)*, 2016: IEEE, pp. 1-6, doi: 10.1109/ITEC.2016.7520272.

[9] H. Zhang, F. Lu, H. Hofmann, W. Liu, and C. C. Mi, "A four-plate compact capacitive coupler design and LCL-compensated topology for capacitive power transfer in electric vehicle charging application," *IEEE Transactions on Power Electronics*, vol. 31, no. 12, pp. 8541-8551, 2016, doi: 10.1109/TPEL.2016.2520963.

[10] E. Abramov, I. Zeltser, and M. M. Peretz, "A network-based approach for modeling resonant capacitive wireless power transfer systems," *CPSS Transactions on Power Electronics and Applications*, vol. 4, no. 1, pp. 19-29, 2019, doi: 10.24295/CPSSTPEA.2019.00003.

[11] M. P. Theodoridis, "Effective capacitive power transfer," *IEEE Transactions on Power Electronics*, vol. 27, no. 12, pp. 4906-4913, 2012, 10.1109/TPEL.2012.2192502.

[12] J. Dai and D. C. Ludois, "Capacitive power transfer through a conformal bumper for electric vehicle charging," *IEEE Journal of Emerging and Selected Topics in Power Electronics*, vol. 4, no. 3, pp. 1015-1025, 2015, doi: 10.1109/JESTPE.2015.2505622.

[13] S. Sinha, B. Regensburger, K. Doubleday, A. Kumar, S. Pervaiz, and K. K. Afridi, "High-power-transfer-density capacitive wireless power transfer system for electric vehicle charging," in *2017 IEEE energy conversion congress and exposition (ECCE)*, 2017: IEEE, pp. 967-974, doi: 10.1109/ECCE.2017.8095890.

[14] B. Regensburger, J. Estrada, A. Kumar, S. Sinha, Z. Popović, and K. K. Afridi, "High-performance capacitive wireless power transfer system for electric vehicle charging with enhanced coupling plate design," in *2018 IEEE energy conversion congress and exposition (ECCE)*, 2018: IEEE, pp. 2472-2477, doi: 10.1109/ECCE.2018.8557881.

[15] F. Lu, H. Zhang, and C. Mi, "A two-plate capacitive wireless power transfer system for electric vehicle charging applications," *IEEE Transactions on Power Electronics*, vol. 33, no. 2, pp. 964-969, 2017, doi: 10.1109/TPEL.2017.2735365.

[16] S. Zou, J. Lu, A. Mallik, and A. Khaligh, "Bi-directional CLLC converter with synchronous rectification for plug-in electric vehicles," *IEEE Transactions on Industry Applications*, vol. 54, no. 2, pp. 998-1005, 2017, doi: 10.1109/TIA.2017.2773430.

[17] V.-B. Vu, M. Dahidah, V. Pickert, and V.-T. Phan, "An improved LCL-L compensation topology for capacitive power transfer in electric vehicle charging," *IEEE Access*, vol. 8, pp. 27757-27768, 2020, doi: 10.1109/ACCESS.2020.2971961.

[18] Z. U. Zahid, Z. Dalala, and J.-S. J. Lai, "Design and control of bidirectional resonant converter for Vehicle-to-Grid (V2G) applications," in *IECON 2014-40th Annual Conference of the IEEE Industrial Electronics Society*, 2014: IEEE, pp. 1370-1376, doi: 10.1109/IECON.2014.7048680.

[19] J.-H. Jung, H.-S. Kim, M.-H. Ryu, and J.-W. Baek, "Design methodology of bidirectional CLLC resonant converter for high-frequency isolation of DC distribution systems," *IEEE Transactions on Power Electronics*, vol. 28, no. 4, pp. 1741-1755, 2012, doi: 10.1109/TPEL.2012.2213346.

[20] J. Min and M. Ordonez, "Bidirectional resonant CLLC charger for wide battery voltage range: Asymmetric parameters methodology," *IEEE Transactions on Power Electronics*, vol. 36, no. 6, pp. 6662-6673, 2020, doi: 10.1109/TPEL.2020.3033982.

[21] S. Toofan, B. Fathipour, and E. Babaei, "A Single Switch Transformer-Less DC-DC Converter with Continuous Input Current for Photovoltaic Applications," *International Journal of Industrial Electronics Control and Optimization*, 2024, doi: 10.22111/ieco.2024.48295.1548.

[22] S. Hasanpour and K. Yari, "A Minimum Phase DC-DC Converter with Continuous Input Current and High Voltage Gain," *International Journal of Industrial Electronics Control and Optimization*, 2024, doi: 10.22111/ieco.2024.48842.1572.

[23] J. Shahsevani and R. Beiranvand, "A Bidirectional Resonant Converter for Capacitive Power Transmission in Electric Vehicle and PowerWall Applications," in *2023 31st International Conference on Electrical Engineering (ICEE)*, 2023: IEEE, pp. 264-270, doi: 10.1109/ICEE59167.2023.10334783.

[24] S. Harini, N. Chellammal, and C. B. Ramesh, "Power flow and reliability analysis of a non-isolated PV/grid connected quasi resonant converter for off-board EV charging station," *International Journal of Modelling and Simulation*, 2024.

[25] F. Nasr Esfahani, A. Darwish, and X. Ma, "Design and Control of a Modular Integrated On-Board Battery Charger for EV Applications with Cell Balancing," *Batteries*, vol. 10, no. 1, p. 17, 2024.

[26] H. Sarnago and Ó. Lucía, "Design and Experimental Verification of a Bidirectional EV On-Board Charger Featuring Multi-Phase Operation in Full Power/Voltage Ranges," *IEEE Open Journal of the Industrial Electronics Society*, 2024, doi: 10.1109/OJIES.2024.3406732.

[27] S.-T. Wu and Y.-W. Chiu, "Implementation of a Bidirectional 400–800V Wireless EV Charging System,"

*IEEE Access*, vol. 12, pp. 26667-26682, 2024, doi: 10.1109/ACCESS.2024.3366997.

[28] R. Patel and C. K. Panigrahi, "GaN based isolated bidirectional multiport DC-DC converter for electric vehicle charging," *e-Prime-Advances in Electrical Engineering, Electronics and Energy*, vol. 8, p. 100574, 2024, doi: 10.1016/j.prime.2024.100574.

[29] Y. Yue, Y. Liu, J. Zhang, H. Zhao, and J. Yang, "Hybrid Control Method of Full-Bridge LLC Resonant Converter Based on Electric Vehicle," *IEEE Access*, 2024.

[30] R. Gopalasami and B. Chokkalingam, "A photovoltaic-powered modified multiport converter for an EV charger with bidirectional and grid connected capability assist PV2V, G2V, and V2G," *World Electric Vehicle Journal*, vol. 15, no. 1, p. 31, 2024, doi: 10.3390/wevj15010031.

[31] Z. Gholami, R. Ildarabadi, H. Heydari-Doostabad, M. Monfared, and T. O'Donnell, "Bidirectional wide range and high voltage gain buck-boost DC-DC converter for EV chargers empowering V2G-G2V applications," *IET Power Electronics*, vol. 17, no. 2, pp. 230-250, 2024.

[32] D. Pesantez, H. Renaudineau, S. Rivera, A. Peralta, A. Marquez Alcaide, and S. Kouro, "Transformerless partial power converter topology for electric vehicle fast charge," *IET Power Electronics*, vol. 17, no. 8, pp. 970-982, 2024.

[33] W. M. Utomo and A. A. Bakar, "Power converter for battery charger of electric vehicle with controllable charging current," *International Journal of Power Electronics and Drive Systems (IJPEDS)*, vol. 15, no. 2, pp. 968-977, 2024, doi: 10.11591/ijpeds.v15.i2.pp968-977.

[34] S. Hu, X. Li, and A. K. Bhat, "Operation of a bidirectional series-resonant converter with minimized tank current and wide ZVS range," *IEEE Transactions on Power Electronics*, vol. 34, no. 1, pp. 904-915, 2018, doi: 10.1109/TPEL.2018.2818145.

[35] Y. Zuo, X. Pan, and C. Wang, "A Reconfigurable Bidirectional isolated LLC Resonant Converter for Ultra-Wide Voltage-gain Range applications," *IEEE Transactions on Industrial Electronics*, 2021, doi: 10.1109/TIE.2021.3088355.

[36] K. Colak, E. Asa, M. Bojarski, and D. Czarkowski, "A novel LLC resonant converter with semi bridgeless active rectifier," in *2014 IEEE Transportation Electrification Conference and Expo (ITEC)*, 2014: IEEE, pp. 1-6, doi: 10.1109/ITEC.2014.6861808.

[37] X. Tang, Y. Xing, H. Wu, and J. Zhao, "An improved LLC resonant converter with reconfigurable hybrid voltage multiplier and PWM-plus-PFM hybrid control for wide output range applications," *IEEE Transactions on Power Electronics*, vol. 35, no. 1, pp. 185-197, 2019, doi: 10.1109/TPEL.2019.2914945.

**Jasem Shahsevani** received his M.Sc. degree in power electronics engineering from Tarbiat Modares University, Tehran, Iran, in 2023. His current research interests include DC/DC converter, LLC-based resonant converter, Grid-Connected inverters, wireless power transfer, electric vehicle charging, soft-switching techniques, and PV-based renewable energy systems.

**Reza Beiranvand** received the MSc and PhD degrees in electrical engineering from Sharif University of Technology, Tehran, Iran, in 1999 and 2010, respectively. From 2010 to 2012, he was a Postdoctoral research fellow with the Electrical Engineering College, Sharif University of Technology. From 1999 to 2007, he was an engineer at the R&D centers of PARS-Electric and RADIO SHAHAB MFGs, Tehran, Iran, where he was engaged in designing the LCD, and LED TVs based on the ST, LT, NXP, and Fairchild devices.

He is currently Head of the Power Electrical Department and Associate Professor with the Faculty of Electrical and Computer Engineering, Tarbiat Modares University, Tehran, Iran. His research interests include power electronics converters, soft switching techniques, SCCs, SMPS, Capacitive-Coupling Power Transfer and Inductive Power Transfer techniques, and PV-based renewable energy systems.

Dr. Beiranvand was the IEEE Consultant (2017-2019), Head of the Power Electrical Department (2018-2020), and Founder of the Power Electronics Converters Lab. of the Tarbiat Modares University. He is between the top 2 % scientists of the world, based on the Stanford University; Stanford, CA, USA released lists, 2020-2024.